

Simultaneous Estimation of Left Ventricular Motion and Material Properties with *Maximum a Posteriori* Strategy

Huafeng Liu and Pengcheng Shi
Department of Electrical and Electronic Engineering
Hong Kong University of Science and Technology
Clear Water Bay, Kowloon, Hong Kong

Abstract

In addition to its technical merits as a challenging non-rigid motion and structural integrity analysis problem, quantitative estimation of cardiac regional functions and material characteristics has significant physiological and clinical values. We have earlier developed a stochastic finite element framework for the simultaneous estimation of myocardial motion and material parameters from medical image sequences with an extended Kalman filter approach. In this paper, we present a new computational strategy for the framework based upon the maximum a posteriori estimation principles, realized through the extended Kalman smoother, that produce a sequence of kinematics state and material parameter estimates from the entire sequence of observations. The system dynamics equations of the heart is constructed using a biomechanical model with stochastic parameters, and the tissue material and deformation parameters are jointly estimated from the periodic imaging data. Experiments with canine magnetic resonance images have been conducted with very promising results, as validated through comparison to the histological staining of post mortem myocardium.

1. Introduction

1.1 Cardiac Motion Analysis

Acute and chronic myocardial ischemia can be identified and localized through the detection of morphological and kinematic abnormalities of the left ventricle (LV) [13]. Accordingly, there have been abundant efforts to analyze cardiac motion and deformation from medical image sequences [6]. Imaging-derived salient features of the LV have been used to establish correspondences between cardiac image frames, including the implanted physical markers [10], the crossings of magnetic resonance (MR) tagging images [20], and the geometrically significant shape landmarks [24]. In order to recover dense field motion/deformation of the entire myocardium from these sparsely matched points, assumptions must be made about

the myocardial behavior in order to constrain the ill-posed problem for a unique solution. Popular strategies include the uses of mathematically motivated regularization [20] and continuum mechanics based models [19, 23].

Because of the periodic nature of the heart motion, the importance of multi-frame analysis is well recognized. Assuming elliptic trajectories of cardiac tissue elements, a Kalman filter framework was constructed to estimate LV deformation from MRI phase contrast velocity fields constrained by segmented myocardial contours [15]. A global geometrical evolution analysis, followed by regional shape matching, was tested on simulated and real endocardial surfaces [3]. And an adaptive filtering scheme with spatial-temporal smoothness and periodicity constraint was proposed to track myocardial contour motion [14].

Conjugate to biomechanics efforts, all image analysis works are based on the premise that mechanical or other constraining models are known as prior information, and the task is to use these models to help estimating kinematics parameters in some optimal sense. The selection of an appropriate model with proper parameters thus largely determines the quality of the analysis results.

1.2 Myocardium Material Characterization

More fundamentally, it has been recognized that alterations in myocardial fiber structure and material elasticity are related to various cardiac pathologies [25], and there have been many works focusing on describing myocardial material characteristics from the biomechanics community [10] and from the medical imaging community [5, 16].

In biomechanics studies of cardiac mechanics and material properties, the kinematics of the heart tissues is assumed to be known from implanted markers or imaging means. The issue is then to use these kinematic observations to estimate material parameters of the constitutive laws. While most works deal with regional finite deformations measured at isolated locations which are then used to arrive at suitable constitutive relationships [11, 12], MR tagging has been used more recently for the *in vivo* study of

the mechanics of the entire heart [5], where unknown material parameters are determined for an exponential strain energy function that maximizes the agreement between the observed (from MR tagging) and the predicted (from finite element modeling) regional wall strains. However, it is recognized that the recovery of kinematics from MR tagging or other imaging techniques is not a solved problem yet, and constraining models of mechanical nature may be needed for the kinematics recovery in the first place [6].

More recently, magnetic resonance elastography (MRE) provides quantitative image of soft tissue material stiffness by processing the displacements resulting from actuating the tissue and using MR imaging techniques to measure the tissue displacements [16]. The technology is still under development, and so far there have been only *in vitro* experiments on soft tissue elasticity measurement. No possibility for *in vivo* MRE of myocardium is at sight.

1.3 Joint Motion and Material Estimation

We have developed the first attempt of simultaneous joint estimation of myocardial kinematics functions and material model parameters based on a stochastic finite element framework [22]. The biomechanical model parameters and the imaging data are treated as random variables with known prior statistics in the dynamic system equations of the left ventricle, and the extended Kalman filter (EKF) procedures are adopted to linearize the augmented state equations and to provide the joint estimates in the least-mean-square sense. This framework is not restricted to any particular imaging data, and experiments have been conducted with MR tagging and MR phase contrast images.

In this paper, we present a new computational strategy for our multi-frame joint estimation framework. The cardiac kinematics (displacement fields and strains) and material (parameters of constitutive laws) properties are recovered using the Bayesian estimation principles. We have employed the extended Kalman smoother (EKS) as the *maximum a posteriori* (MAP) state and parameter sequence estimator. That is, we compute the most likely estimates that best describe the observed data as a whole. This way, we avoid the possible divergence problem of the EKF approach by employing forward and backward filtering to obtain improved averaged estimates.

We realize that several efforts in recursive structure and motion estimation from images are of relevance to our work. An EKF strategy was used for recursive recovery of motion, pointwise structure, and focal length from feature correspondence tracked through an image sequence [1]. A particle-filter like expectation maximization (EM) framework, based on the CONDENSATION algorithm, was developed for non-Gaussian observations and multi-class dynamics [18]. And EM/EKS is adopted to impose time-

continuity of estimated motion parameters in [21]. Our work differs from these in the sense that it is constrained by biomechanically motivated system dynamics, and we are explicitly dealing with non-rigid object with much increased complexity.

2. LV System Dynamics

2.1 Biomechanical Model of the Myocardium

The biomechanical model of the myocardium implicitly regularizes the dynamic behavior of the heart. In order to construct a realistic yet computationally feasible analysis framework using imaging data and other available measurements, the structure, dynamics, and material of the left ventricle should be properly modeled. In general, the heart is a non-rigid object that deforms over time and has very complicated biomechanical properties in terms of the constitutive laws [10]. For computational simplicity, we adopt the isotropic linear elastic model for the myocardium in our current implementation, where the stress σ and strain ε relationship obeys the Hooke's law:

$$\sigma = S\varepsilon \quad (1)$$

More realistic models, such as the transversely isotropic material [10] which accounts for the preferential stiffness in the myofiber directions (the fiber stiffness is about 1.5 to 3 times greater than the cross-fiber stiffness in normal cases), can be easily adopted for the three-dimensional analysis if the myofiber structure is available from the myofiber model [17] or from diffusion tensor magnetic resonance images (DTMRI) [7]. However, since the presented framework is for 2D case, we use the linear material model to illustrate the basic ideas and rationales of a novel joint estimation strategy. Assuming the displacement along the x - and y -axis of a point to be $u(x, y)$ and $v(x, y)$ respectively, the infinitesimal strain tensor ε of the point can be expressed as:

$$\varepsilon = \begin{bmatrix} \frac{\partial u}{\partial x} & \frac{\partial v}{\partial y} \\ \frac{\partial u}{\partial y} + \frac{\partial v}{\partial x} \end{bmatrix} \quad (2)$$

and under plane strain condition, matrix S is:

$$S = \frac{E}{(1+\nu)(1-2\nu)} \begin{bmatrix} 1-\nu & \nu & 0 \\ \nu & 1-\nu & 0 \\ 0 & 0 & \frac{1-2\nu}{2} \end{bmatrix} \quad (3)$$

Here, E and ν , the *Young's modulus* and the *Poisson's ratio*, are two material-specific constants we want to estimate. Currently, the material parameter priors are derived from literatures on post mortem tissue testing [26], while their distributions over a large population are unknown.

2.2 Stochastic Finite Element Method

The stochastic finite element method (SFEM) is used for the representation of the LV structure and dynamics. SFEM has been used for structural dynamics analysis in probabilistic frameworks [4], where structural material properties are described by random fields, possibly with known prior statistics, and the observations and loads are treated as noise-corrupted. This way, stochastic differential dynamics equations are combined with the finite element method to study the dynamic structures with uncertainty in their parameters and measurements.

In our 2D implementation, a Delaunay triangulated finite element mesh is formed (Fig. 3), bounded by endocardial and epicardial boundaries. An isoparametric formulation defined in a natural coordinate system is used, where, for tri-nodal linear element, the basis functions are linear functions of the nodal coordinates [2]. We arrive at the following system dynamics equation of the LV:

$$M\ddot{U} + C\dot{U} + KU = R \quad (4)$$

where M , C and K are the mass, damping and stiffness matrices, R the load vector, and U the displacement vector. Because the myocardium density is generally considered to be uniform, M is a known function of the material density and is temporally and spatially constant. K is a function of the material constitutive law, and is related to the material-specific Young's modulus and Poisson's ratio, which vary temporally and spatially. In our framework, these two local material parameters are treated as random variables with known *a priori* statistics, and will be estimated along with the motion functions. (Please note that currently we do not consider the temporal dependency of the material parameters). C is frequency dependent, and we assume Rayleigh damping with $C = \alpha M + \beta K$. In practice, it is difficult to determine the damping parameters because they are frequency dependent, and we assume Rayleigh damping for the very low damping heart tissue and fix the two weighting constants to be 1%. These two parameters can actually be put into our augmented state vectors and be estimated from our framework as well.

2.3 State Space Representation

Since we have employed the linear material model, Eqn. 4 can be transformed into a state-space representation of a continuous-time linear stochastic system:

$$\dot{x}(t) = A_c(\theta)x(t) + B_c w(t) \quad (5)$$

where the material parameter vector θ , the state vector x , the system matrices A_c and B_c , and the control (input) term

w are:

$$\theta = \begin{bmatrix} E \\ \nu \end{bmatrix}, \quad x(t) = \begin{bmatrix} U(t) \\ \dot{U}(t) \end{bmatrix}, \quad w(t) = \begin{bmatrix} 0 \\ R(t) \end{bmatrix}$$

$$A_c = \begin{bmatrix} 0 & I \\ -M^{-1}K & -M^{-1}C \end{bmatrix}$$

$$B_c = \begin{bmatrix} 0 & 0 \\ 0 & M^{-1} \end{bmatrix}$$

An associated measurement equation, which describes the observed imaging data $y(t)$, can be expressed in the form:

$$y(t) = Dx(t) + e(t) \quad (6)$$

where D is a known measurement matrix, and $e(t)$ is the measurement noise.

In our framework, Eqns. 5 and 6 represent a continuous-time system with discrete-time measurements, or a so-called sampled data system. The input term, available from pressure measurements or computed from the system equation using the initial conditions, is piecewise constant over the sampling interval T . Implicitly assuming hidden Markov model for the state equations, we arrive at the discrete dynamics equation [9]:

$$x((k+1)T) = Ax(kT) + Bw(kT) \quad (7)$$

with $A = e^{A_c T}$ and $B = A_c^{-1}(e^{A_c T} - I)B_c$. For general continuous-time system with discrete-time measurements, including the process noise $v(t)$, we have the state equation:

$$x(t+1) = A(\theta)x(t) + B(\theta)w(t) + v(t) \quad (8)$$

2.4 Augmented State Space Representation

The myocardial dynamics and observations are now represented by Eqns. 6 and 8. This representation provides a natural framework for the biomechanics study of myocardium material constitutive laws with observations/measurements on the kinematics states, and for the physically-motivated image analysis of cardiac kinematics properties with assumed biomechanical constraining models. However, in practice, neither the kinematics data nor the model parameters are precisely known. We have proposed a SFEM framework where the data and the model parameters are treated as random variables, possibly with known or assumed prior distributions, to determine the best estimates of the spatial distributions of the material parameters and the spatial-temporal kinematics parameters simultaneously [22].

In order to perform the joint estimation, the *unknown* state vector x is augmented by the *unknown* material parameter vector θ to form the new state vector $z = [x \ \theta]^T$, and we have the new pair of augmented state/measurement equations:

$$z(t+1) = f(z(t), w(t)) + v_s(t) \quad (9)$$

$$y(t) = h(z(t)) + e_o(t) \quad (10)$$

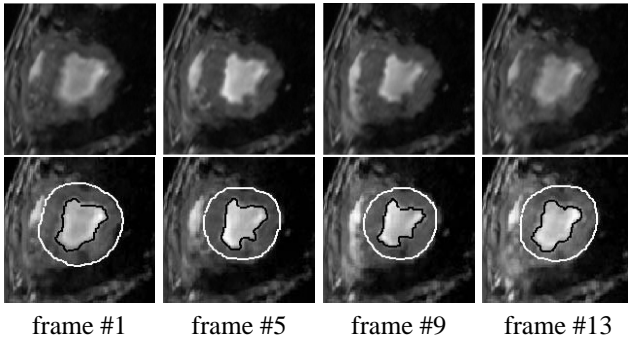


Figure 1: Canine cardiac MR images.

where

$$f(z(t), w(t)) = \begin{bmatrix} A(\theta)x(t) + B(\theta)w(t) \\ \theta \end{bmatrix}$$

$$h(z(t)) = \begin{bmatrix} D & 0 \end{bmatrix} \begin{bmatrix} x(t) \\ \theta(t) \end{bmatrix}$$

$$v_s(t) = \begin{bmatrix} v(t) \\ 0 \end{bmatrix}, \quad e_o(t) = \begin{bmatrix} e(t) \\ 0 \end{bmatrix}$$

The joint state and parameter estimation problem can be understood as a state estimation problem for this nonlinear system. Assuming known Gaussian augmented process and measurement noises:

$$v_s(t) \sim N(0, Q_s), \quad Q_s = \begin{bmatrix} Q_v & 0 \\ 0 & 0 \end{bmatrix}$$

$$e_o(t) \sim N(0, R_o), \quad R_o = \begin{bmatrix} R_e \\ 0 \end{bmatrix}$$

this form of formulation leads to a solution of the filtering problem using the extended Kalman filter (EKF) framework, which is based on linearization of the augmented state equations at each time step. A recursive procedure with natural block structure is used to perform the joint state (kinematics) and parameter (material) estimation [22]. The Gaussian assumptions are convenient for the filtering framework, and their variances would determine the applicability of the framework to LV of different states of health.

3. The Maximum A Posteriori Estimation Strategy

We aim to estimate a dense displacement field and material parameters distribution from the entire imaging/imaging derived data, which corresponds to maximize the posterior probability density function with the model parameter $p(z|y)$. Here, we employ the EKS as the maximum *a posteriori* (MAP) state and parameter sequence estimator. This way, a Bayesian estimation framework allows us to combine the statistical likelihood in terms of probability density

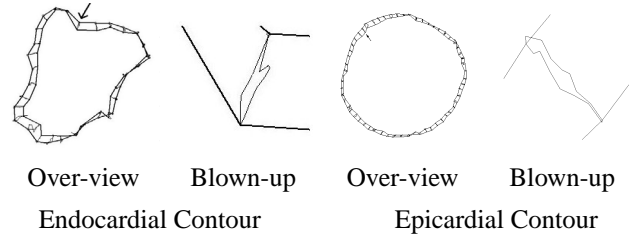


Figure 2: Boundary displacement constraints throughout the cardiac cycle at selected endo- and epi-cardial points.

function (PDF) of the state and observation with a continuum biomechanics constraining model, using a state space representation of the system dynamics. It should be noted here that we can incorporate any model parameters into the augmented state z , such as the uncertain noise properties, without losing any generality of our approach.

3.1 Basic Concepts

With the Bayes' rule, we have:

$$\hat{z} = \arg \max_z \{p(z|y) = \frac{p(z, y)}{p(y)}\} \quad (11)$$

We note that $p(y)$ is a constant once the measurements have been made and can therefore be ignored in the maximization process. Then maximizing the posterior PDF $p(z|y)$ is equivalent to maximize the joint PDF $p(z, y)$. This can be achieved by an EKS based estimation framework.

Assuming the prior distribution on the initial augmented state $z(0)$ is Gaussian white with mean \hat{z}_0 and covariance Σ_0 :

$$p(z(0)) = \frac{\exp\{-\frac{1}{2}[z(0) - \hat{z}_0]^T Q_s^{-1}[z(0) - \hat{z}_0]\}}{2\pi|\Sigma_0|^{\frac{1}{2}}} \quad (12)$$

We construct the PDF of $z(t)$ given $z(t-1)$:

$$p(z(t)|z(t-1)) = \frac{\exp\{-\frac{1}{2}[z(t) - f(t-1)]^T Q_s^{-1}[z(t) - f(t-1)]\}}{2\pi|Q_s|^{\frac{1}{2}}} \quad (13)$$

and the conditional PDF of $y(t)$ given $z(t)$:

$$p(y(t)|z(t)) = \frac{\exp\{-\frac{1}{2}[y(t) - h(z(t))]^T R_o^{-1}[y(t) - h(z(t))]\}}{2\pi|R_o|^{\frac{1}{2}}} \quad (14)$$

where $f(t-1) = f(z(t-1), w(t-1))$, and $|Q_s|$ and $|R_o|$ are the determinants of matrix Q_s and R_o respectively.

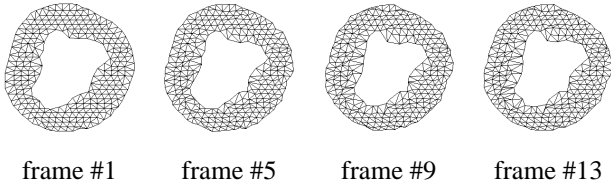


Figure 3: Estimated deforming meshes.

3.2 Likelihood Function

Denote a sequence of observations $Y = [y(1), \dots, y(N)]$ and augmented system states $Z = [z(1), \dots, z(N)]$, where N is the total number of image frames, $z(t)$ is the state of all the myocardial points (fixed number) at frame t , and $y(t)$ all the observations (varying size due to the time-dependent imaging data) at frame t . By the Markov property implied by our state model, the joint likelihood for Z and Y is:

$$p(Z, Y) = \prod_{t=1}^N p(y(t)|z(t)) \prod_{t=1}^N p(z(t)|z(t-1))p(z(0)) \quad (15)$$

The MAP estimates of the augmented state vector Z are the solutions to the maximization problem:

$$\max_Z \{ \ln p(Z, Y) \} \quad (16)$$

Expanding and rearranging the terms in Eqn. 15, we have

$$\begin{aligned} \max_Z \{ & - \sum_{t=1}^N (\frac{1}{2} [y(t) - h(z(t))]^T R_o^{-1} [y(t) - h(z(t))]) \\ & - \sum_{t=1}^N (\frac{1}{2} [z(t) - f(t-1)]^T Q_s^{-1} [z(t) - f(t-1)]) \\ & - \frac{1}{2} [z(0) - \hat{z}_0]^T \Sigma_0^{-1} [z(0) - \hat{z}_0] \\ & - \frac{N}{2} \ln |R_o| - \frac{N}{2} \ln |Q_s| - \frac{1}{2} \ln |\Sigma_0| + Const \} \quad (17) \end{aligned}$$

3.3 The Extended Kalman Smoother Algorithm

There are several ways to maximize the log-likelihood function of Eqn. 17. A recursive method is the extended Kalman smoother, which can be used to approximate $\hat{z}(t)$ by linearization of the system around the current state estimation. It can take advantages of periodic nature of the heart motion and we can cyclically feed the updated image and image derived data into our framework until reaching convergence. The EKS can be realized by the forward extended Kalman filter followed by a backward smoothing filter [8].

Like a Taylor series, we can linearize the estimation around the current estimate using the partial derivatives of

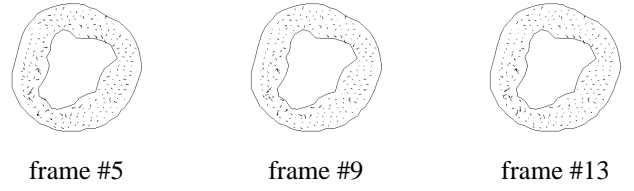


Figure 4: Estimated displacement maps (vs. frame # 1).

the process and measurement functions to compute estimates even in the face of non-linear relationships. The operation of the EKF is the same one as the linear Kalman filter, which adopts a form of feedback control in estimation: the filter estimates the process state at some time and then obtains feedback in the form of measurements. As such, the equations for the EKF fall into two groups: time update equations and measurement update equations. The time update equations are responsible for projecting forward the current state and error covariance estimates to obtain the *a priori* estimates for the next time step, while the measurement update equations are responsible for the feedback.

The forward extended Kalman filter is initialized with $\hat{z}(0) = \hat{z}_0$ and $P(0) = \Sigma_0$, and the state estimates and their error covariance matrices are computed sequentially, using:

1. Project the state ahead

$$\hat{z}^-(t) = f(\hat{z}(t-1), w(t)) \quad (18)$$

2. Project the error covariance ahead

$$P^-(t) = F_t P(t-1) F_t^T + Q_s \quad (19)$$

3. Compute the Kalman Gain

$$G(t) = P^-(t) H^T (H P^-(t) H^T + R_o)^{-1} \quad (20)$$

4. Update the estimate with measurement

$$\hat{z}(t) = \hat{z}^-(t) + G(t)(z(t) - h(\hat{z}^-(t))) \quad (21)$$

5. Update the error covariance

$$P(t) = (I - G(t)H)P^-(t) \quad (22)$$

with

$$\begin{aligned} F_t &= \left. \frac{\partial}{\partial z} f(z(t), w(t)) \right|_{z=\hat{z}} \\ &= \begin{bmatrix} A(\hat{\theta}) & M_t \\ 0 & I \end{bmatrix} \\ H(\hat{z}(t)) &= \left. \frac{\partial}{\partial z} h(z(t)) \right|_{z=\hat{z}} = [D \ 0] \\ M_t &= \left. \frac{\partial}{\partial \theta} (A(\theta)\hat{x}(t) + B(\theta)w(t)) \right|_{\theta=\hat{\theta}} \\ P(0) &= \begin{bmatrix} P_1(0) & P_2(0) \\ P_2^T(0) & P_3(0) \end{bmatrix} \end{aligned}$$

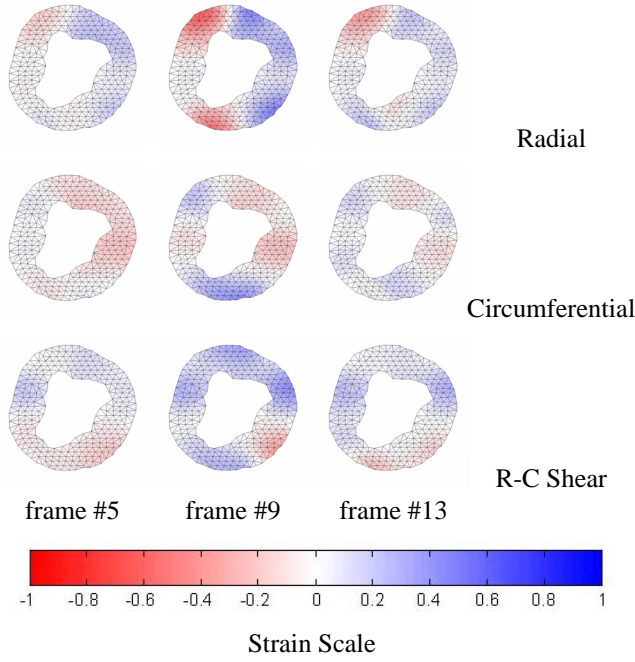


Figure 5: Estimated radial, circumferential, and R-C shear strain maps (vs. frame # 1).

Here, $P_1(0)$ is the kinematics state error covariance sub-matrix which is related to our confidence measure on the input imaging data (see next section on the construction of confidence measures for shape-based boundary displacements used in our experiments), $P_3(0)$ is the material parameter covariance sub-matrix whose values are proportional to the possible knowledge of the myocardium under study, and $P_2(0)$ is the kinematics-material correlation sub-matrix with zero entries.

The backward smoothing of the EKS is achieved through the well-known Rauch-Tung-Striebel smoother [8],:

$$\Lambda(t) = P(t)F_t^T P^-(t+1) \quad (23)$$

$$\hat{z}(t|T) = \hat{z}(t) + \Lambda(t)(\hat{z}(t+1|T) - \hat{z}^-(t+1)) \quad (24)$$

4. Experiments

4.1 Imaging Data

Canine experiment was conducted, where a hydraulic occluder was used to produce a controlled, graded coronary stenosis in the central left anterior descending (LAD) coronary artery territory. Sixteen canine MR images are acquired over the heart cycle, with imaging parameters flip angle = 30° , $TE = 34msec$, $TR = 34msec$, $FOV = 28cm$, $5mm$ skip 0, matrix 256×128 , 4 nex, $venc = 15cm/sec$.

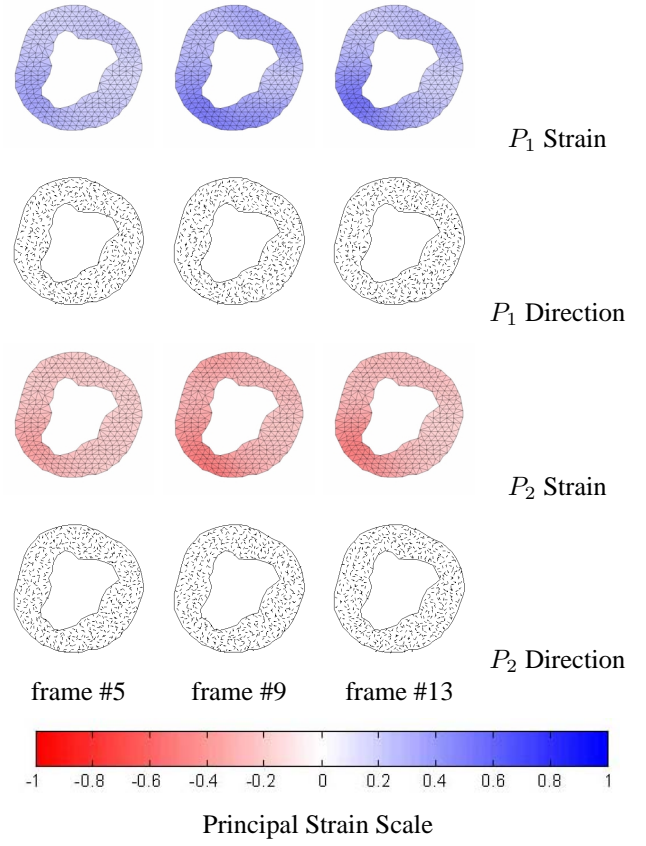


Figure 6: Estimated principal strain and associated direction maps (vs. frame # 1).

The spatial resolution is $1.09mm/pixel$, and the temporal resolution is $31.25msec/frame$. Fig.1 shows the examples of the images from the sequence and the detected endocardial and epicardial boundaries.

4.2 Inputs for the Framework

Boundary displacements between consecutive frames are detected based on locating and matching geometric landmarks and a local coherent smoothness model [24]. Based on the hypothesis that the LV boundary contours deform as little as possible between successive temporal frames, bending energy measure is used as the matching criterion to obtain the point correspondences between contours:

$$\min_{\varphi \in \mathcal{C}} e_{bend}(\phi, \varphi) = \min_{\varphi \in \mathcal{C}} [\kappa_f(\phi) - \kappa_s(\varphi)]^2 \quad (25)$$

where $\kappa_f(\phi)$ is the curvature for a point ϕ in the first contour, \mathcal{C} the corresponding search region on the second contour, and $\kappa_s(\varphi)$ the curvature of a candidate point φ within the search region. Among all the candidate points, the one at ξ which yields the smallest bending energy is chosen as

the matched point, and the bending energy value indicates the goodness $m_g(\xi) = e_{bend}(\phi, \xi)$ of the match.

Further, the bending energy measures for all other points within the search region are recorded as the basis to measure the uniqueness of the matching choice. Ideally, the bending energy value of the chosen point should be an outlier (much smaller value) compared to the values of the rest of the candidate points. If we denote the mean value of the bending energy measures of all the points inside the search window except the chosen point as \bar{e}_{bend} and the standard deviation as σ_{bend} , we define the uniqueness measure of the match as:

$$m_u(\xi) = \left| \frac{e_{bend}(\phi, \xi)}{\bar{e}_{bend} - \sigma_{bend}} \right| \quad (26)$$

Obviously for both goodness and unique measures, the smaller the values the more reliable the match. Combining these two together, we arrive at a *confidence measure* for the matched second contour point ξ of the first contour point ϕ :

$$c(\xi) = \frac{1}{k_{1,g} + k_{2,g}m_g(\xi)} \frac{1}{k_{1,u} + k_{2,u}m_u(\xi)} \quad (27)$$

where $k_{1,g}$, $k_{2,g}$, $k_{1,u}$, and $k_{2,u}$ are normalizing constants such that the confidence measures for all point matches between contours are in the range of 0 to 1.

This process yields a set of shape-based, best-matched displacement vectors for each pair of contours, and each vector has an associated confidence measure. Elements of the kinematics error covariance sub-matrix $P_1(0)$ will be weighted by $(1 - c(\xi))$. Fig. 2 shows the displacement trajectories for the endo- and epicardial points throughout the cardiac cycle, and these displacements and their associated confidences are used as the initial kinematics states and the initial covariance matrix entries. Appropriate covariance matrices play essential roles in determining the sensible/converged outputs, as it is well known that the major disadvantage of any Kalman strategies is the required detail priors on the noise statistics.

Based on biomechanics testing of canine myocardium [26], the initial Young's modulus and Poisson ratio are set to 75000 Pascal and 0.47, with initial variance 200 and 0.001, respectively. In order to handle large discontinuities of the material parameters, which if directly imposed may require prior knowledge on the pathological conditions of the tissue elasticity, we have utilized a strategy by updating the material priors for the next iteration with the current estimates and the original variances for the first a few loops of the computation. This enables the handling of a much wider range of material variations.

4.3 Results

In the reported real image experiment, the LV slice consists of 295 nodes and 500 elements. On a P4 1.8GHz PC and

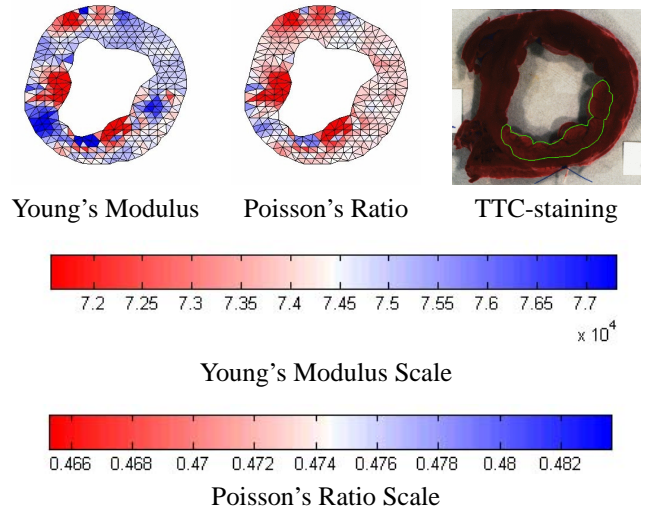


Figure 7: Estimated material parameter maps and the highlighted TTC-stained post mortem myocardium.

under Matlab 6.0, it took ~ 40 minutes for each loop and 10 loops for the system to converge. Under C++ environment, the processing time is reduced to ~ 40 minutes in total.

Fig. 3 shows the original LV mesh at end-diastole (ED) and the selected meshes (frames #5, #9, and #13) estimated from the framework. The corresponding displacement maps are shown in Fig. 4, the cardiac-specific radial (R), circumferential (C), and R-C shear strain maps are shown in Fig. 5, and the principal strains and their associated principal directions are shown in Fig. 6.

The final converged estimates of the Young's modulus and Poisson's ratio distributions and mapping scales are presented in Fig. 7, as well as the highlighted histological results of triphenyl tetrazolium chloride (TTC) stained post mortem myocardium, often considered the gold-standard. Spatially, the Young's modulus varies from 71500 to 77500 *Pascal*, and the Poisson ratio varies from 0.465 to 0.483. While meaningful interpretation of these material parameter results is still underway, it is obvious that the material parameters seem more sensitive than the kinematics results (displacement and strains) to differentiate the transmural properties, which are considered the key indications for early detection of ischemic pathologies.

5. Summary and Conclusions

In this paper, we have described an MAP based estimation framework for multi-frame joint estimation of cardiac kinematics and material properties from medical image sequence. Here, this approach adopts material models with random field parameters, and using EKS to estimate motion, deformation and material parameters simultaneously. This non-invasive joint estimation strategy offers new possibili-

ties to study myocardial kinematics and material characteristic from a variety of imaging data, and early experiments have shown that material parameters have better sensitivity for transmural properties than motion parameters. Efforts on adopting particle filter and H_∞ filter are in progress, which can deal with global minimum issue and noise characteristics issue respectively.

Acknowledgments

Thanks to Dr. Albert Sinusas of Yale University for the canine experiments and the imaging data. This work is supported by HKRGC-CERG HKUST6057/00E.

References

- [1] A. Azarbayejani and A.P. Pentland. Recursive estimation of motion, structure and focal length. *IEEE Transactions on Pattern Analysis and Machine Intelligence*, 17:562–575, 1995.
- [2] K. Bathe and E. Wilson. *Numerical Methods in Finite Element Analysis*. Prentice-Hall, New Jersey, 1976.
- [3] P. Clarysse, D. Friboulet, and I.E. Magnin. Tracking geometrical descriptors on 3-D deformable surfaces - application to the left-ventricular surface of the heart. *IEEE Transactions on Medical Imaging*, 16:392–404, 1997.
- [4] H. Contreras. The stochastic finite element method. *Computers and Structures*, 12:341–348, 1980.
- [5] L.L. Creswell, M.J. Moulton, S.G. Wyers, J.S. Pirolo, D.S. Fishman, W.H. Perman, K.W. Myers, R.L. Actis, M.W. Vannier, B.A. Szabo, and M.K. Pasque. An experimental method for evaluating constitutive models of myocardium in *in vivo* hearts. *American Journal of Physiology*, 267:H853–H863, 1994.
- [6] A.J. Frangi, W.J. Niessen, and M.A. Viergever. Three-dimensional modeling for functional analysis of cardiac images: A review. *IEEE Transactions on Medical Imaging*, 20(1):2–25, 2001.
- [7] L. Geerts, P. Bovendeerd, K. Nicolay, and T. Arts. Characterization of the normal cardiac myofiber field in goat measured with MR-diffusion tensor imaging. *American Journal of Physiology*, 283(1):H139–H145, 2002.
- [8] A. Gelb. *Applied Optimal Estimation*. MIT Press, Cambridge, MA, 1974.
- [9] T. Glad and L. Ljung. *Control Theory*. Taylor & Francis, London, 2000.
- [10] L. Glass, P. Hunter, and A. McCulloch. *Theory of Heart*. Springer-Verlag, New York, 1991.
- [11] J.M. Guccione, A.D. McCulloch, and L.K. Waldman. Passive material properties of intact ventricular myocardium determined from a cylindrical model. *Journal of Biomechanical Engineering*, 113:42–55, 1991.
- [12] P.J. Hunter and B.H. Smaill. The analysis of cardiac function: a continuum approach. *Progress in Biophysics and Molecular Biology*, 52:101–164, 1989.
- [13] M.J. Lipton, J. Bogaert, L.M. Boxt, and R.C. Reba. Imaging of ischemic heart disease. *European Radiology*, 12:1061–1080, 2002.
- [14] J.C. McEachen, A. Nehorai, and J.S. Duncan. Multiframe temporal estimation of cardiac nonrigid motion. *IEEE Transactions on Image Processing*, 9:651–665, 2000.
- [15] F.G. Meyer, R.T. Constable, A.J. Sinusas, and J.S. Duncan. Tracking myocardial deformation using spatially constrained velocities. *IEEE Transactions on Medical Imaging*, 15(4):453–465, 1996.
- [16] R. Muthupilla, D.J. Lomas, P.J. Rossman, J.F. Greenleaf, A. Manduca, and R.L. Ehman. Magnetic resonance elastography by direct visualization of propagating acoustic strain waves. *Science*, 269(5232):1854–1857, 1995.
- [17] P.M. Nielsen, I.J. LeGrice, B.H. Smaill, and P.J. Hunter. Mathematical model of geometry and fibrous structure of the heart. *American Journal of Physiology*, 260(4):H1365–H1378, 1991.
- [18] B. North, A. Blake, M. Isard, and J. Rittscher. Learning and classification of complex dynamics. *IEEE Transactions on Pattern Analysis and Machine Intelligence*, 22:1016–1034, 2000.
- [19] X. Papademetris, A.J. Sinusas, D.P. Dione, R.T. Constable, and J.S. Duncan. Estimation of 3-D left ventricular deformation from medical images using biomechanical models. *IEEE Transactions on Medical Imaging*, 21(7):786–799, 2002.
- [20] J. Park, D.N. Metaxas, and L. Axel. Analysis of left ventricular wall motion based on volumetric deformable models and MRI-SPAMM. *Medical Image Analysis*, 1:53–71, 1996.
- [21] Y.D. Seo and K.S. Hong. Structure and motion estimation with expectation maximization and extended kalman smoother for continuous image sequences. In *Computer Vision and Pattern Recognition I*, pages 1148–1154, 2001.
- [22] P. Shi and H. Liu. Stochastic finite element framework for cardiac kinematics function and material property analysis. In *Medical Image Computing and Computer Assisted Intervention*, pages 634–641, 2002.
- [23] P. Shi, A. Sinusas, R. T. Constable, and J. Duncan. Volumetric deformation analysis using mechanics-based data fusion: Applications in cardiac motion recovery. *International Journal of Computer Vision*, 35(1):87–107, 1999.
- [24] P. Shi, A. Sinusas, R. T. Constable, E. Ritman, and J. Duncan. Point-tracked quantitative analysis of left ventricular motion from 3D image sequences. *IEEE Transactions on Medical Imaging*, 19(1):36–50, 2000.
- [25] S.A. Wickline, E.D. Verdonk, A.K. Wong, R.K. Shepard, and J.G. Miller. Structural remodelling of human myocardial tissue after infarction: quantification with ultrasonic backscatter. *Circulation*, 85:269–268, 1992.
- [26] H. Yamada. *Strength of Biological Material*. The Williams and Wilkins Company, Baltimore, 1970.